Soheyl	Massoudi	soheyl.massoudi@epfl.ch
First	*Last*	*email*

ASME Paper Title: Robust Design of Herringbone Grooved Journal Bearings using Multi-Objective Optimization with Artificial Neural Networks

Authors: Soheyl Massoudi, Jürg Schiffmann

ASME Journal Title: Proceedings of the ASME Turbo Expo 2023: Turbomachinery Technical Conference and Exposition

Volume/Issue 13D Date of Publication (VOR* Online) September 28, 2023

ASME Digital Collection URL: https://asmedigitalcollection.asme.org/GT/proceedings-abstract/GT2023/87110/1168655

DOI: https://doi.org/10.1115/GT2023-102428

*VOR (version of record)

Proceedings of the ASME Turbo Expo 2023
Turbomachinery Technical Conference and Exposition
GT2023
June 26-30, 2023, Boston, Massachusetts

GT2023-102428

ROBUST DESIGN OF HERRINGBONE GROOVED JOURNAL BEARINGS USING MULTI-OBJECTIVE OPTIMIZATION WITH ARTIFICIAL NEURAL NETWORKS

Soheyl Massoudi[1,*], Jürg Schiffmann[1]

[1]Laboratory for Applied Mechanical Design
Ecole Polytechnique Fédérale de Lausanne (EPFL)
CH-1015 Lausanne, Switzerland

ABSTRACT

Herringbone grooved journal bearings (HGJBs) are widely used in micro-turbocompressor applications due to their high load-carrying capacity, low friction, and oil-free solution. However, the performance of these bearings is sensitive to manufacturing deviations, which can lead to significant variations in their performance and stability. In this study, design guidelines for robust design against manufacturing deviations of HGJB supported micro-turbocompressors are proposed. These guidelines are based on surrogate model assisted multi-objective optimization using ensembles of artificial neural networks trained on a large dataset of rotor and bearing designs as well as operating conditions. The developed framework is then applied to a series of case studies representative of heat-pump and fuel cell micro-turbomachines. To highlight the importance of rotor geometry and bearing aspect ratio in the robustness of HGJBs, two types of optimizations are performed: one focusing on optimizing the bearing geometry, and the other focusing on both the bearing and rotor geometries. The analysis of the Pareto fronts and Pareto optima of each type of optimization and case study allows for the derivation of design guidelines for the robust design of HGJB supported rotors. Results suggest that by following these guidelines, it is possible to significantly improve the robustness of herringbone grooved journal bearings against manufacturing deviations, resulting in stable operation. The best design achieved $\pm 8\,\mu\text{m}$ *tolerance on the bearing clearance, and designs optimized for both rotor and bearing geometry outperformed those optimized for bearing geometry alone. This work successfully identifies guidelines for the robust design of herringbone grooved journal bearings in micro-turbocompressor applications, demonstrating the strength of surrogate model assisted multi-objective optimization. It provides a valuable tool for engineers seeking to optimize the performance and reliability of these bearings.*

Keywords: Herringbone grooved journal bearings, gas-bearings, micro-turbomachinery, manufacturing deviations, multi-objective optimization, artificial neural networks, surrogate model

*Corresponding author: soheyl.massoudi@epfl.ch

NOMENCLATURE

Roman letters

A	Bearing front
B	Bearing rear
D	Bearing diameter [m]
f	Objective function/Performance metric [context dependent unit]
F	Force [N]
G	Geometry field [context dependent unit]
h_g	Groove depth [m]
h_r	Ridge clearance [m]
HV	Measure of feasible region [context dependent unit]
I	Moment of inertia [kg m^2]
k	Sweep sampling [−]
L	Bearing axial length [m]
L_A	Bearing front to center of gravity midplane distance [m]
L_B	Bearing rear to center of gravity midplane distance [m]
M	Rotor mass [kg]
N	Rotational speed [RPM]
P	Pressure [Pa]
R	Bearing radius [m]
S/N	Signal-to-Noise ratio [−]
S	Search space
$\dot{E}$	Losses [W]

Greek letters

α	Groove-ridge width ratio [−]
β	Groove angle [°]
γ	Grooved region ratio [−]
Γ	Logarithmic decrement [−]

Δ	Variation of a given variable
θ	Circumferential coordinate [°]
Λ	Compressibility number [−]
μ	Viscosity [Pa s]
ρ	Density [kg m^{-3}]
Ω	Angular velocity [rad s^{-1}]

Superscripts and subscripts

a	ambient
ex	excitation frequency
exp	centrifugal expansion
F	feasible
g	groove
i	i_{th} element
nom	nominal
p	polar
r	ridge
rob	robust
rot	rotor
t	transverse
w	weight
¯	Dimensionless/Mean

Acronyms

ANN	Artificial Neural Network
CG	Center of Gravity
GA	Genetic Algorithm
GPGPU	General Purpose Graphics Processing Unit
HGJB	Herringbone Grooved Journal Bearing
LHS	Latin Hypercube Sampling
NGT	Narrow Groove Theory
NSGA	Non dominated Sorting Genetic Algorithm

1. INTRODUCTION

1.1 Nature of the Issue

Herringbone grooved journal bearings (HGJBs) are commonly designed using multi-objective optimization to achieve optimal nominal design values for maximizing both the logarithmic decrement and load capacity [1]. However, the performance of gas lubricated bearings is known to be highly sensitive to manufacturing deviations, which can impact the stability, load capacity, and losses of the bearings [2]. Therefore, a mathematical definition that accounts for these sensitivities and that allows identifying the range of the feasible region is necessary to assess the robustness of a specific design [3].

Although multi-objective optimization is a common practice in bearing design [4], it has limitations as it does not guarantee the minimization of gradients of the figure of merit or symmetry of the feasible region around the nominal point. To address these limitations and to design more robust ball bearings, Verma and Tiwari [5] used a single-objective optimization approach that maximized the dynamic capacity and minimized its variation, expressed as a first-order Taylor expansion, using a genetic algorithm. This approach works, however, only if the response surface of the selected performance metrics is convex and continuous. One of the main challenges to assessing the robustness of gas-bearing supported rotors is the non-convex and discontinuous response surface of the rotordynamic stability as a function of geometrical deviation. This calls for a large sampling around a nominal design point to assess the robustness, which can become very time-consuming in a multi-objective optimization setting. Guenat and Schiffmann [6] partially addressed this issue by developing an approach that is based on a normalized multidimensional look-up table based on the bearing critical mass as a metric for stability. While being very fast and efficient, the critical mass based approach does not allow capturing the full rotordynamic behavior of gas-bearing supported rotors. To address this issue, the idea here is to capitalize on prior work by Massoudi et al. [7] who implemented an artificial neural network (ANN) based optimization framework for the robust design of centrifugal compressors.

Considering the low number of published data on robust design of gas lubricated bearings, there is a lack of design guidelines for the robust design of gas-bearing supported rotors that consider the full modeling of the rotor and bearings.

1.2 Goals and Objectives

The objectives of this study are (1) the application of previously developed robustness metrics and of a surrogate model assisted multi-objective optimization framework to the design of gas-bearing supported rotors, (2) design guidelines for robust HGJB supported rotors, and (3) the generalization of these results using proper dimensionless variables for the design of HGJB supported rotors against manufacturing deviations.

1.3 Scope of the Paper

The aim of this study is to utilize advanced modeling techniques and optimization tools to derive design guidelines for robust HGJB supported rotors that are resilient to manufacturing deviations. The idea is to use the trained surrogate model to construct a global model of the rotordynamics of HGJB supported rotors. The use of ensembles of artificial neural networks allows for the construction of an accurate global model, which can be implemented on general purpose graphics processing units (GPGPUs) to reduce the computation time.

The global model and the robustness metrics are used to formulate a multi-objective optimization approach for the robust design of HGJB supported rotors under constraints. The quality of the resulting designs will be evaluated using the proposed robustness metrics. The proposed optimization approach will be applied to the design of HGJBs for use in micro-turbocompressors. The results of the optimization are then generalized based on a minimal subset of dimensionless variables that drive the rotordynamics equations. This allows for the design of HGJB supported rotor against manufacturing deviations.

2. THEORY

2.1 Surrogate Model Definition

The baseline model used for this work is based on a gas-bearing supported rotor model developed by Schiffmann and Favrat [8]. Figure 1 shows the HGJB supported turbocompressor system under study, while Fig. 2 illustrates the bearing parameters, such as groove width (a), ridge width (b), bearing length (L), ungrooved length (L_{land}), groove depth (h_{g}), and local bearing clearance (h_{r}). The distances L_{A} and L_{B} indicate the distance from each bearing's center plane to the turbocompressor's center

of gravity. The baseline model solves the rotordynamic equations of motion of a 4 degrees of freedom rigid rotor supported on two equivalent herringbone grooved journal bearings. The bearing is modeled using the Narrow Groove Theory (NGT), which assumes an infinite number of grooves [9]. The combination of the thin film assumptions and the NGT leads to a modified Reynolds-equation that captures the effects of the grooves on the fluid film behavior. That equation is then linearized via perturbation, and the bearing impedances (stiffness and damping matrices) are extracted for the rotordynamic calculations. A detailed overview of the modeling approaches has been introduced by Gu et al. [10], and an experimental validation is given by Guenat and Schiffmann [11]. The logarithmic decrement measures rotor system stability, calculated by the ratio of imaginary to real parts of eigenvalues at excitation frequencies that match imaginary parts. A positive value indicates stability. Rotor and bushings are treated as rigid, and four modes are excited: cylindrical forward/backward, conical forward/backward. The surrogate model is trained using Latin hypercube sampling (LHS) generated data from the baseline model.

Iseli and Schiffmann [12] identified a minimal set of dimensionless groups governing the dynamics of gas-bearing supported rotors. This study adopts a modified version of their subset, normalized by bearing length to connect the dimensionless groups of the bearing to those of the rotor. The surrogate model takes 11 dimensionless groups as input (Tab. 1) and outputs a categorical variable to detect an eigenmode, another to determine stability, and dimensionless values for whirl speed ratio (Ω_{ex}/Ω), and logarithmic decrement (Γ). The surrogate model, developed by Massoudi and Schiffmann [13], utilizes feed-forward artificial neural networks with regression and binary classification networks. The model employs an averaging ensemble technique using six different weight initialization methods for improved accuracy, which are He Normal, Lecun Normal, Glorot Uniform, He Uniform, Lecun Uniform, and Glorot Normal [14–17]. The final prediction is the average of the predictions from the six neural networks. To optimize the hyperparameters, a genetic algorithm (GA) is used to minimize loss, measured by the mean absolute error for regressors and categorical cross-entropy for classifiers [18]. This procedure is performed for all ANNs, and is computationally intensive, so to reduce the burden, each ANN's gradient descent is set to 5 epochs, and the GA is set to 5 generations with an initial population of 100.

To evaluate a nominal rotor design's robustness, a parameter sweep is conducted for the rotational speed N and micrometer-scale manufacturing parameters, such as the groove depth h_g and the radial bearing clearance h_r, which are crucial for assessing stability. A sweep in N is also necessary to check for excitation during acceleration. The resulting array of designs and operating conditions is combined with other nominal rotor designs and used as input to the surrogate model, which predicts the whirl-speed ratio and logarithmic decrement for each of the four eigenmodes of the rotor. The minimum value of the logarithmic decrements is used to assess the rotor system's stability. Finally, the feasible region of each rotor is evaluated with respect to manufacturing deviations under optimization constraints.

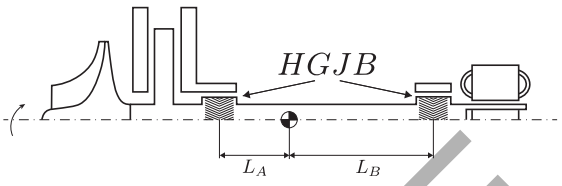

FIGURE 1: VISUALIZATION OF THE TURBOCOMPRESSOR SUPPORTED BY HERRINGBONE GROOVED JOURNAL BEARINGS.

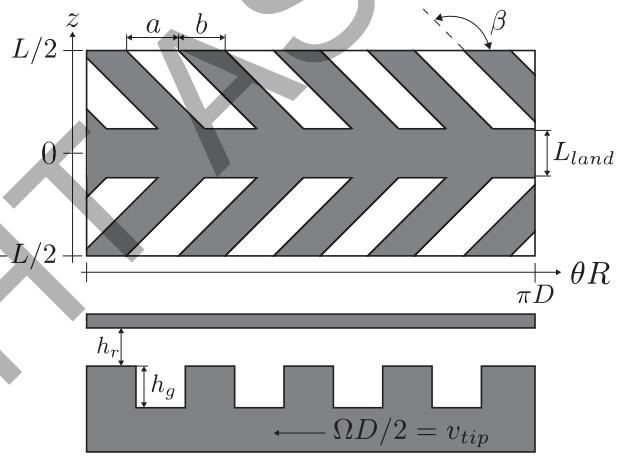

FIGURE 2: UNWRAPPED TOP AND CUT VIEWS OF THE HERRINGBONE GROOVED JOURNAL BEARING (HGJB) AND ITS PARAMETERS.

2.2 Definition of Robustness

The robustness of gas-bearing supported rotors is evaluated using two metrics. The first metric, HV, represents the fraction of the sampled region around the nominal point that is feasible under manufacturing deviations and applied optimization constraints (see Fig. 3). Robustness evaluation leads to a feasible domain defined by S_F under deviations of g_1 and g_2 by Δg_1 and Δg_2 from their nominal values $g_{1,\text{nom}}$ and $g_{2,\text{nom}}$, respectively. Outside of S_F, the design constraints are no longer respected. The second metric, S/N, is the signal-to-noise ratio, which measures the decline of performance metrics such as stability, load capacity, or efficiency across the feasible region. It is calculated over the feasible region defined by HV for the logarithmic decrement (a metric of stability), the load capacity, and the bearings losses. It is defined in Eq. (1) for a performance metric f to maximize and in Eq. (2) for a performance metric f to minimize, where μ is the mean and σ^2 the variance. Since S/N is always maximized in the optimization, the two definitions are formulated to ensure

TABLE 1: SET OF DIMENSIONLESS VARIABLES USED AS INPUT TO THE ENSEMBLES OF ARTIFICIAL NEURAL NETWORKS

Variable	Symbol
Groove-ridge width ratio	$\alpha = \frac{a}{a+b}$
Groove angle	β
Grooved region ratio	$\gamma = \frac{L-L_{\text{land}}}{L}$
Bearing length to diameter ratio	$LoD = \frac{L}{2R}$
Ratio of bearings distances to CG	$H_{\text{gr}} = 1 + \frac{h_{\text{g}}}{h_{\text{r}}}$
Mass number	$\overline{M} = \frac{M h_{\text{r}} \Omega^2}{P_{\text{a}} R^2}$
Transverse moment of inertia number	$\overline{I_{\text{t}}} = \frac{I_{\text{t}} h_{\text{r}} \Omega^2}{P_{\text{a}} R^2 L^2}$
Polar moment of inertia number	$\overline{I_{\text{p}}} = \frac{I_{\text{p}} h_{\text{r}} \Omega^2}{P_{\text{a}} R^2 L^2}$
Bearing A distance to CG	$\overline{L_{\text{A}}} = \frac{L_{\text{A}}}{L}$
Bearing B distance to CG	$\overline{L_{\text{B}}} = \frac{L_{\text{B}}}{L}$
Compressibility number	$\Lambda = \frac{6 \cdot \mu \Omega \cdot (D/2)^2}{P_{\text{a}} \cdot h_{\text{r}}^2}$

that μ is either maximized or minimized, and that σ^2 is always minimized. The average $\overline{S/N}$ of the signal-to-noise ratio for the stability, losses and load capacity of the HGJB is used as an optimization objective.

$$S/N_{\text{f}} = 10 \cdot \log_{10}\left(\frac{\mu_{\text{f}}^2}{\sigma_{\text{f}}^2}\right) \tag{1}$$

$$S/N_{\text{f}} = -10 \cdot \log_{10}\left(\mu_{\text{f}}^2 + \sigma_{\text{f}}^2\right) \tag{2}$$

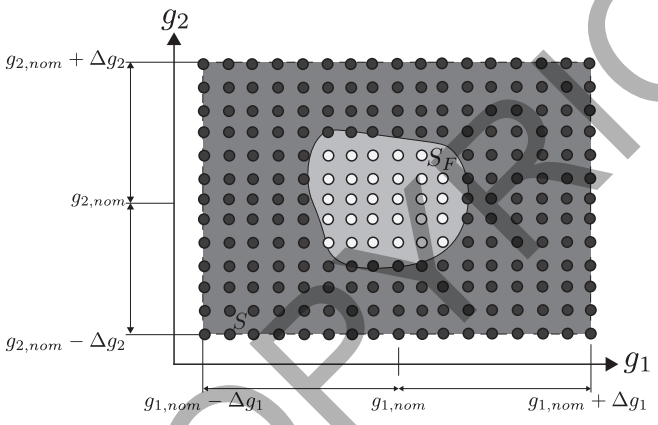

FIGURE 3: THE FEASIBLE DOMAIN IS DEFINED BY S_{F}, WHICH IS ROBUST TO DEVIATIONS OF g_1 AND g_2 FROM THEIR NOMINAL VALUES BY Δg_1 AND Δg_2, RESPECTIVELY. DESIGN CONSTRAINTS ARE NOT SATISFIED OUTSIDE OF S_{F}. *HV* IS COMPUTED AS THE RATIO OF SAMPLES SATISFYING THE CONSTRAINTS IN WHITE TO THE TOTAL NUMBER OF SAMPLES.

2.3 Surrogate Model Assisted Optimization

The sensitivity analysis around the nominal point requires a large number of samples, increasing the computational effort. To reduce this computation time, a global surrogate model made of ensembles of artificial neural networks is used. ANNs take advantage of the high degree of parallelism and high memory bandwidth of graphics processing units (GPUs) to speed up the computation. Neural network algorithms are well suited for GPU hardware because they typically involve large and numerous buffers of parameters, activation values, and gradient values, which are large enough to fall outside the cache of a central processing unit (CPU). As a result, the surrogate model allows for the efficient evaluation of the numerous samples generated by the robust optimization at each generation of the algorithm.

The search for the optimal robust design is driven by an evolutionary algorithm. Through successive generations of the algorithm, designs that maximize or minimize the selected optimization objectives are favored, ultimately leading to a Pareto front. We also apply a selection process to retain only those designs that satisfy the design constraints. Depending on the algorithm, constraints may be relaxed or dominated designs may be retained through intermediate generations to favor diversity and ensure a better exploration of the design space.

3. METHODS

3.1 Multi-Objective Optimization Setup

The geometries of the HGJBs and rotor are optimized using a multi-objective optimization approach. The two bearings are identical and the design variables explored are listed in Tab. 2. The Non-dominated Sorting Genetic Algorithm III (NSGA-III) [19, 20], a widely used evolutionary algorithm for multi-objective optimization, was implemented in Python for this purpose [21]. An adaptive-operator selection procedure, which is a technique used to improve the efficiency of the optimization process by adapting the selection of genetic operators to the characteristics of the problem [22, 23], was also used. A set of uniformly sampled reference directions, as proposed by Das and Dennis [24], were used to guide the optimization process over 250 generations.

TABLE 2: DESCRIPTION OF THE PARAMETERS FOR THE MULTI-OBJECTIVE OPTIMIZATION

Term	Symbol	Range/Value	Unit
HGJB Variables			
Groove-ridge width ratio	α	0.32–0.68	–
Groove angle	β	-167.5 – -122.5	°
Grooved land region ratio	γ	0.52 – 0.97	–
Groove depth	h_{g}	$2.5 \cdot 10^{-6}$ – $28.5 \cdot 10^{-6}$	m
Local bearing clearance	h_{r}	$2.5 \cdot 10^{-6}$ – $28.5 \cdot 10^{-6}$	m
Rotor Variables			
Rotor segment lengths	L_{i}	$2 \cdot 10^{-3}$ – $100 \cdot 10^{-3}$	m
Fixed parameters			
h_{g} deviations[1]	Δh_{g}	$4 \cdot 10^{-6}/8 \cdot 10^{-6}$	m
h_{r} deviations[2]	Δh_{r}	$4 \cdot 10^{-6}$ /$8 \cdot 10^{-6}$	m
Robustness sampling unit	k_{rob}	7	–
Speed sampling sweep	k_{N}	5	–

Two optimization types were defined. In the first type, identified as "H", only the bearing geometry was optimized, with the bearing aspect ratio LoD and the rest of the rotor geometry fixed.

[1] ±8 µm deviations on h_{g} for R1/H1 only, 4 µm otherwise.
[2] ±8 µm deviations on h_{r} for R1/H1 only, 4 µm otherwise.

The first objective is the maximization of HV to obtain the largest feasible region. The second objective is the maximization of the mean signal-to-noise ratio $\overline{S/N}$. It is computed by taking the average of the signal-to-noise ratio of Γ, F and $\dot{E}_{\mathrm{HGJB}}$. In the second type, named "R", both the bearing geometry including LoD and the length of the rotor can vary, subject to the constraint that the initial design length was not exceeded. The objectives for this optimization were the same as for the first type, with the addition of minimizing the rotor shaft windage losses $\dot{E}_{\mathrm{rot}}$. The objectives and constraints for the optimization of the bearings-rotor geometry are defined in Eq. (3).

$$
\begin{aligned}
\max_{G_{\mathrm{HGJB}},\, G_{\mathrm{ROT}}} \quad & (HV, \overline{S/N}, -\dot{E}_{\mathrm{rot}}) \\
\text{s.t.} \quad & v_{\mathrm{tip}} < 250\,\mathrm{m\,s^{-1}}, \\
& F_{\mathrm{L,10kRPM}} > 1.20 \cdot F_{\mathrm{W}}, \\
& \Delta h_{\mathrm{r,exp}} < 2\,\mu\mathrm{m}, \\
& \mathbf{GA} \cdot \mathbf{GB} < 0, \\
& \Gamma > 0.1, \\
& HV > 0.3, \\
& L_{\mathrm{rot}} < L_{\mathrm{rot,i}} + 3\,\mathrm{mm}, \\
& \overline{L_{\mathrm{A}}} > 0.5, \\
& \overline{L_{\mathrm{B}}} > 0.5, \\
& \dot{E}_{\mathrm{HGJB}} < 300\,\mathrm{W}, \\
& \Lambda < 60, \\
& \Omega_{\mathrm{ex,cyl_F}} > \Omega_{\mathrm{ex,cyl_B}}, \\
& \frac{\partial^2 \Omega_{\mathrm{ex,cyl_F}}}{\partial N^2} < 0, \\
& \frac{\partial \Omega_{\mathrm{ex,cyl_F}}}{\partial N} > 0
\end{aligned}
\tag{3}
$$

with

v_{tip} : the tip velocity at the radial bearings
F_{W} : the weight of the system
$F_{\mathrm{L,10kRPM}}$: the lift force delivered by a radial bearing
$\Delta h_{\mathrm{r,exp}}$: radial clearance expansion
$\mathbf{GA}$: vector from center of gravity to 1st bearing
$\mathbf{GB}$: vector from center of gravity to 2nd bearing
N : rotational speed
L_{rot} : optimized rotor length
$L_{\mathrm{rot,i}}$: initial rotor length
$\dot{E}_{\mathrm{HGJB}}$: bearing losses
Λ : compressibility number
Γ : logarithmic decrement, metric of stability
$\Omega_{\mathrm{ex,cyl_F}}$: excitation frequency

Among the applied constraints, the tip velocity is limited for structural integrity. A load capacity condition is applied to ensure rotor lift off with a 20% safety factor at a rotor speed of 10 kRPM. The radial expansion is limited to 2 µm to allow for designs with low nominal bearing clearance h_{r}. A constraint is set on the position vectors of the radial bearings with respect to the center of gravity (CG) of the system. Their dot product must be negative to ensure they are on each side of the CG. Only stable nominal designs are selected with a safety margin of 0.1 on the logarithmic decrement Γ. A minimum of 30% of the sampled region is set to be feasible under constraints. $\overline{L_{\mathrm{A}}}$ and $\overline{L_{\mathrm{B}}}$ should be greater than 0.5 to prevent the center of gravity from being positioned on the bearings. Each bearing's loss $\dot{E}_{\mathrm{HGJB}}$ must be less than 300 W to avoid designs that prioritize stability through excessive dissipation. The compressibility number Λ must be kept below 60 to remain within the range of the training data used in the surrogate model. The excitation frequency of the cylindrical forward mode should be greater than that of the cylindrical backward mode for the majority of the sampled points. The last two constraints specify that the cylindrical forward excitation frequency should increase monotonically at a decreasing rate. Constraints are placed on the excitation frequency to avoid designs that are estimated to be very robust by both the baseline model and the surrogate model. Without these constraints, the optimization may converge to a particular type of Pareto optima that consists of designs with the cylindrical forward excitation frequency increasing to a synchronous excitation before suddenly collapsing to a subsynchronous excitation as the rotational speed of the rotor increases. These types of excitation have not been observed experimentally and are thought to be caused by numerical errors due to stiff differential equations in the baseline model or by a Hopf instability. As a result, these designs are avoided in the optimization process.

3.2 Case Studies

Six rotors from different application use cases are analyzed in detail. Their length and bearing outer diameter, as well as mass and moments of inertia are shown in Fig. 4. Each rotor is characterized by an identifying number ranging from 1 to 6. The letters R and H refer to the rotor-bearing optimization and bearing-only optimization respectively. R1/H1 is a test rotor without thrust bearing running in Air. R2/H2 is a heat-pump compressor running in R134a. R3/H3 is a fuel-cell recirculation fan operating in steam. R4/H4-R6/H6 are test rotors to extend the design space and explored operating conditions. Their operating conditions are presented in Tab. 3.

TABLE 3: OPERATING CONDITIONS OF THE TEST ROTORS

Term	Unit	R1	R2	R3	R4	R5	R6
Fluid		Air	Steam	R134a	R134a	Air	Air
P	MPa	0.1	0.125	0.251	0.25	0.1	0.1
T	K	293	685	300	304	290	290
N_{nom}	kRPM	100	260	250	250	120	500

3.3 Estimating Relevant Features for Robust Design

The relevant features for robust designs were assessed statistically. The Pareto fronts of each optimization were compared between H-optimizations and R-optimizations, and between case studies. The original designs, which were mainly obtained through nominal optimizations aimed at maximizing stability, load capacity, and minimizing losses, served as a benchmark for evaluating the improvement achieved by the new method. The distribution of the Pareto optimum design parameters were then

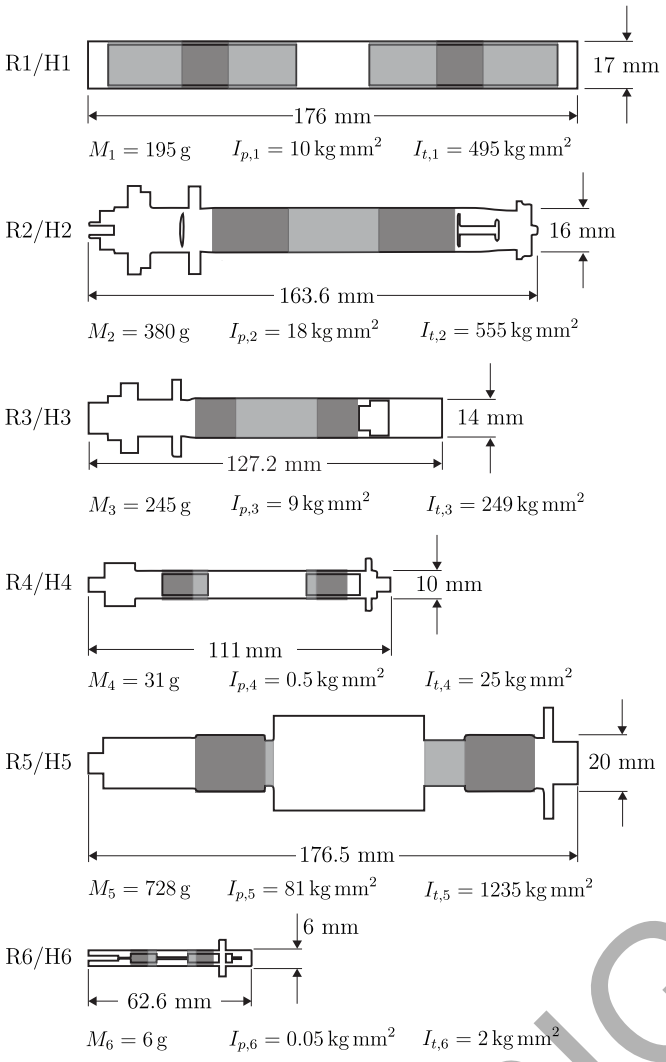

FIGURE 4: MASS, MOMENTS OF INERTIA, LENGTH AND BEARING DIAMETER OF THE ROTORS CONSIDERED IN THIS STUDY. DARKER GREY REGIONS REPRESENT THE HERRINGBONE GROOVED JOURNAL BEARINGS. LIGHT GREY REGIONS ARE THE SEGMENTS BEING OPTIMIZED IN LENGTH IN R-OPTIMIZATIONS. WHITE REGIONS HAVE FIXED GEOMETRY.

analyzed using boxplots. Patterns were searched among the design parameters of the Pareto optima across the optimizations.

4. RESULTS

4.1 Computational Acceleration

An optimization covered a total of 1 239 750 rotor designs for 5 sampled points for speed between 10 kRPM and the corresponding nominal speed, and for 7 sampled points for the bearing clearance and 7 sampled points for the groove depth to assess the robustness. This represents a total of 303 738 750 samples. Each optimization takes about 2h on a desktop computer running an Nvidia Ampere GPU with 10 GB of RAM and 8704 cuda cores.

4.2 Pareto Fronts and Solutions

The Pareto fronts for the rotors, shown in Fig. 5, reveal consistent trade-offs among the different rotor families from R1/H1 to R6/H6. The H-optimization of each case study focuses solely on bearing parameters, except for LoD, while the R-optimization includes both bearing parameters and rotor length. The most robust solutions are identified by selecting those with the highest HV values, which are highlighted with larger markers in the figures. To facilitate the comparison, HV is converted to an area measured by the product of $2\Delta h_\mathrm{r}$ and $2\Delta h_\mathrm{g}$. The results indicate a competition between HV and $\overline{S/N}$, resulting in higher windage losses $\dot{E}_\mathrm{rot}$ when both robustness metrics are simultaneously increased. Notably, rotor 5's original design has a high value of $\alpha = 0.74$, exceeding the search space's predefined bounds, so no solution was found in the H5 optimization. However, all other rotors have Pareto optima in the H-optimizations, with the R-optimizations typically yielding more robust solutions in terms of both HV and $\overline{S/N}$. Rotor 1's robust solution, $\mathrm{R1_{rob}}$, attains the highest HV value of nearly $HV = 228\,\mu\mathrm{m}^2$. The solutions $\mathrm{R2_{rob}}$ and $\mathrm{H2_{rob}}$ exhibit similar robustness characteristics, setting them apart from the other optimized solutions. Finally, the original design solutions are represented by a star marker. They are outperformed by the solutions obtained from the H-optimizations in terms of both robustness metrics (HV and $\overline{S/N}$). Rotor 3's original design has a HV value close to zero due to insufficient load capacity, resulting in minimal stability variation over the small feasible region and a significant increase in the signal-to-noise ratio.

The response surfaces for the R-optimizations and H-optimizations are presented in Fig. 6 and Fig. 9 respectively, showing the stability of the system (logarithmic decrement) with respect to manufacturing deviations. Higher tolerances are targeted for the bearing clearance h_r due to the difficulty of grinding the bearing and its bushing, which can, however, reach $\pm 0.5\,\mu\mathrm{m}$ by investing a significant effort. The laser engraving of grooves reaches an accuracy of $\pm 1\,\mu\mathrm{m}$ on the groove depth with ease.

All of the robust designs yield a large tolerance for deviations in groove depth, with a minimum tolerance of $\Delta h_\mathrm{g} = \pm 3\,\mu\mathrm{m}$. The tolerance for the local bearing clearance, h_r, is more challenging to achieve, but all of the robust R-solutions ($\mathrm{R_{rob}}$) have a tolerance of at least $\Delta h_\mathrm{r} = \pm 2\,\mu\mathrm{m}$, with $\mathrm{R1_{rob}}$ reaching a tolerance of $\Delta h_\mathrm{r} = \pm 8\,\mu\mathrm{m}$ as shown in Fig. 6a. The contour plots are compared with the baseline model to verify the accuracy of the neural network-based surrogate model, suggesting a very good agreement between the two. The slight deviations observed are acceptable and do not affect the conclusions on the robustness of the design.

4.3 Relevant Features for Robust Design

The results of the study are presented as boxplots of the identified Pareto optimal distributions X, with respect to their design variables and objective HV. Figure 7 and Fig. 8 show the solutions found in the R-optimizations and H-optimizations, respectively. The selected robust solutions in each optimization are marked with colored dots. The results show that grooves larger than ridges are favored, with a groove-ridge width ratio $\alpha = 0.68$ for all $\mathrm{R_{rob}}$ solutions, except for $\mathrm{R5_{rob}}$ with $\alpha = 0.52$. This suggests that larger α values could have been selected if the search space boundaries were extended. Values of β are found in a range spanning from $-142°$ to $-136°$. The range of values for the bearing aspect ratio LoD for the selected $\mathrm{R_{rob}}$ solutions is

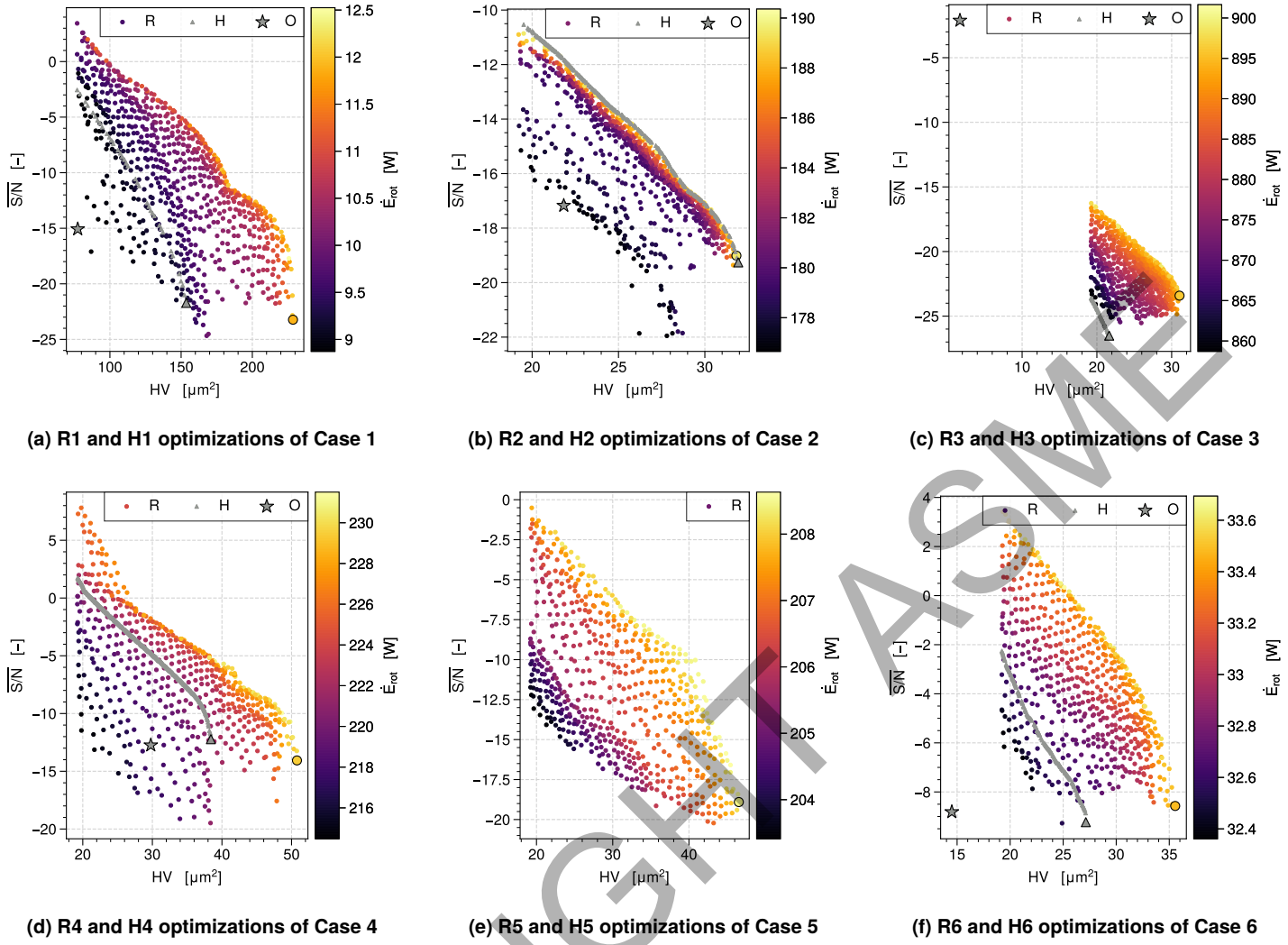

(a) R1 and H1 optimizations of Case 1

(b) R2 and H2 optimizations of Case 2

(c) R3 and H3 optimizations of Case 3

(d) R4 and H4 optimizations of Case 4

(e) R5 and H5 optimizations of Case 5

(f) R6 and H6 optimizations of Case 6

FIGURE 5: PARETO FRONTS OF 12 OPTIMIZATIONS (H-OPTIMIZATION AND R-OPTIMIZATION). OBJECTIVES INCLUDE FEASIBILITY (HV), MEAN SIGNAL-TO-NOISE RATIO ($\overline{S/N}$), AND ROTOR WINDAGE LOSSES ($\dot{E}_{\mathrm{rot}}$). GREY CURVES REPRESENT H-OPTIMIZATIONS, WHILE COLORED FRONTS REPRESENT R-OPTIMIZATIONS. THE ORIGINAL OPTIMIZED SOLUTION IS DENOTED BY A STAR MARKER, WHILE ROBUST SOLUTIONS ARE HIGHLIGHTED BY MARKERS OF LARGER SIZE. H5 YIELDED NO RESULT.

above the third quartile of their respective X_{R} distributions, with values ranging from 1.24 to 1.81. Robust solutions are found in the range of 2.4 to 3.3 for the groove to clearance ratio H_{gr}, which accounts for radial expansion. The dimensionless mass $\overline{M}$ ranges from around 17 to 300 for the selected $\mathrm{R}_{\mathrm{rob}}$ solutions, with the highest value found for X_{R2} and the smallest values for X_{R4}. The selected dimensionless polar moment of inertia $\overline{I_{\mathrm{p}}}$ for all robust solutions are below the first quartile, except for $\mathrm{R2}_{\mathrm{rob}}$, while the dimensionless transverse moment of inertia is above the third quartile for $\mathrm{R2}_{\mathrm{rob}}$ and below the first quartile for all other designs. Only $\mathrm{R1}_{\mathrm{rob}}$ achieves equal dimensionless bearing midplane distance to the center of gravity of the rotor for both directions, while all other robust solutions show an asymmetry. The compressibility numbers for all R-optimizations cover a wide range, from 4.5 for X_{R1} to 60 for X_{R5}, but all $\mathrm{R}_{\mathrm{rob}}$ solutions have compressibility numbers close to the median value of their respective X_{R} distributions.

In the H-optimizations, the robust solutions have fixed aspect ratios LoD that are mainly closer to 1, while in the R-optimizations, they are closer to 2. One exception is observed for $\mathrm{H2}_{\mathrm{rob}}$ with a fixed LoD of 1.75, similar to that of the $\mathrm{R2}_{\mathrm{rob}}$ solution. The groove-ridge width ratio is an important design parameter for the robust solutions. However, the H-optimizations produce solutions with smaller groove angles and lower groove-ridge width ratios compared to the R-optimizations. The $\mathrm{H}_{\mathrm{rob}}$ solutions have a groove depth to bearing clearance ratio in the range of 2.8 to 3.3, which is similar to the $\mathrm{R}_{\mathrm{rob}}$ geometries. The distribution of the groove-ridge width ratio α for the $\mathrm{H}_{\mathrm{rob}}$ solutions do not saturate, with values ranging from 0.44 to 0.68. Lower values of the ratio of grooved region and bearing length γ are also observed in some of the H-optimized designs. The compressibility numbers for the H-optimized solutions are generally higher than the R-optimized solutions, with an exception for $\mathrm{H1}_{\mathrm{rob}}$ and $\mathrm{H4}_{\mathrm{rob}}$.

Overall, the results of both R-optimizations and H-optimizations reveal that there is a trade-off between the aspect

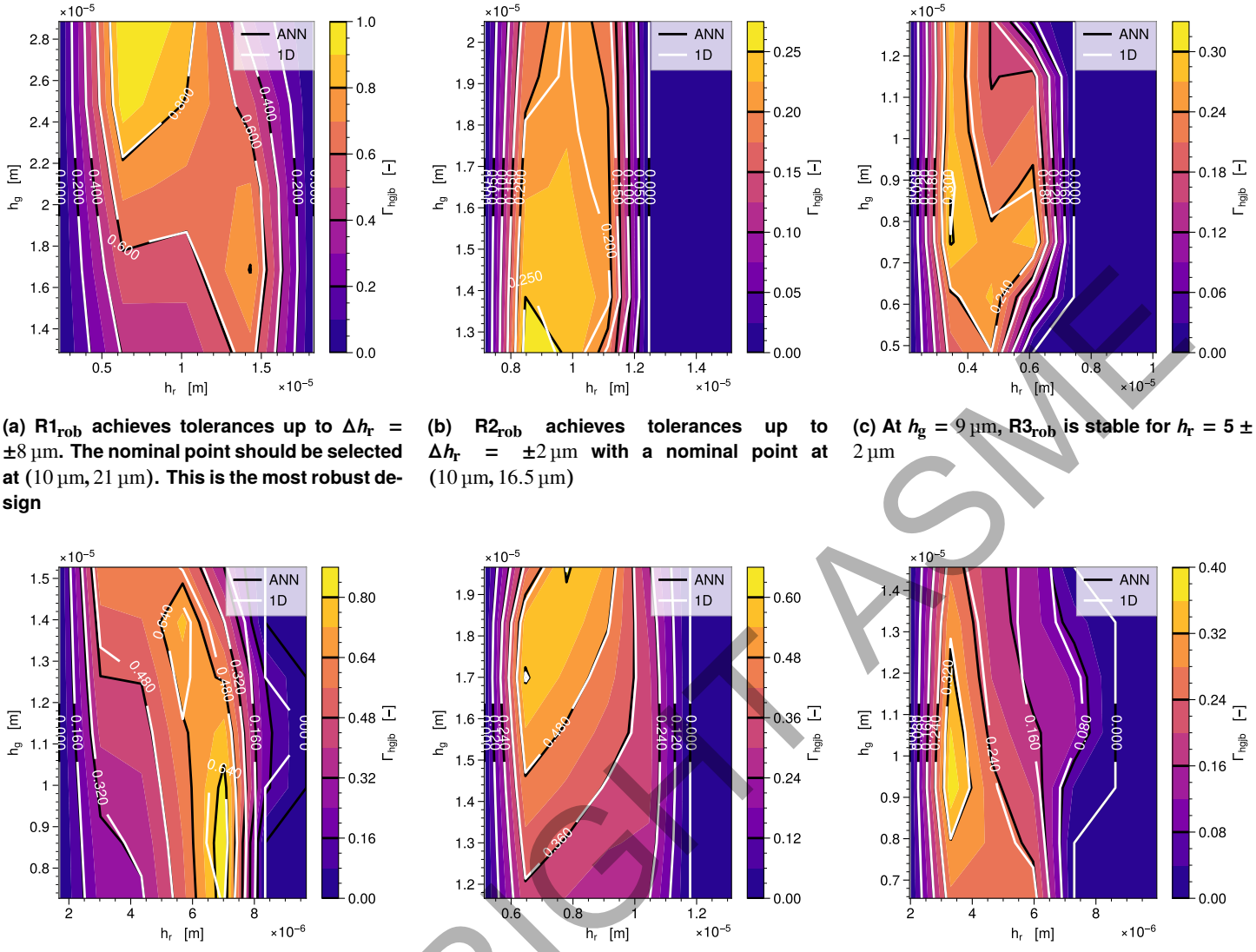

(a) R1$_{rob}$ achieves tolerances up to $\Delta h_r = \pm 8\,\mu m$. The nominal point should be selected at $(10\,\mu m, 21\,\mu m)$. This is the most robust design

(b) R2$_{rob}$ achieves tolerances up to $\Delta h_r = \pm 2\,\mu m$ with a nominal point at $(10\,\mu m, 16.5\,\mu m)$

(c) At $h_g = 9\,\mu m$, R3$_{rob}$ is stable for $h_r = 5 \pm 2\,\mu m$

(d) R4$_{rob}$ comfortably achieves $\pm 2\,\mu m$ on the local bearing clearance at $h_r = 5\,\mu m$ for a groove depth of $h_g = 11.5\,\mu m$

(e) R5$_{rob}$ achieves $\Delta h_r = \pm 2.5\,\mu m$ at $h_r = 8.5\,\mu m$ and $h_g = 15.5\,\mu m$

(f) R6$_{rob}$ with $h_r = 5\,\mu m$ and $h_g = 11\,\mu m$ achieves $\Delta h_r = \pm 2\,\mu m$

FIGURE 6: RESPONSE SURFACES OF ROBUST DESIGNS FOUND IN R-OPTIMIZATIONS, PLOTTED AS A LOGARITHMIC DECREMENT CONTOUR MAP AGAINST MANUFACTURING DEVIATIONS OF h_r AND h_g. DESIGNS WITH A LOGARITHMIC DECREMENT HIGHER THAN 0.1 ARE CONSIDERED STABLE. WHITE CONTOUR LINES ARE EVALUATED WITH THE 1D CODE USED TO TRAIN THE SURROGATE MODEL. ALL ROBUST DESIGNS ACHIEVED AT LEAST $\Delta h_r = \pm 2\,\mu m$.

ratio, the groove-ridge width ratio, and the groove angle. The dimensionless mass and dimensionless polar moment of inertia are not as consistent between the different robust solutions.

5. DISCUSSION

The trade-offs observed on the Pareto fronts were consistent across the rotor families, with H-optimizations representing subset Pareto curves of the R-optimizations. The competition between the two robustness metrics, HV and $\overline{S/N}$, was evident, with increasing feasible region (HV) making it challenging to maintain high $\overline{S/N}$. The rotor length was found to be a critical factor driving the rotor windage losses. Specifically, with fixed diameter and material, longer rotors resulted in higher transverse moment of inertia, polar moment of inertia, and mass. The Pareto fronts for H2 and R2 revealed the crucial role of the bearing aspect ratio (LoD) in achieving robust HGJB rotor designs. The robust solutions identified through the optimization process were superior to the original designs, with the latter being Pareto-dominated even by the solutions of H-optimizations with poor robustness in terms of HV and $\overline{S/N}$.

Robust solutions for herringbone-grooved journal bearings can be designed with a fixed rotor geometry. The design guidelines include selecting groove angles β in a range of $-158°$ to $-154°$ for a fixed LoD of 1. An asymmetrical rotor design with different $\overline{L_A}$ and $\overline{L_B}$ favors lower α values in the range of 0.44 to 0.56 for a less sensitive design to manufacturing deviations.

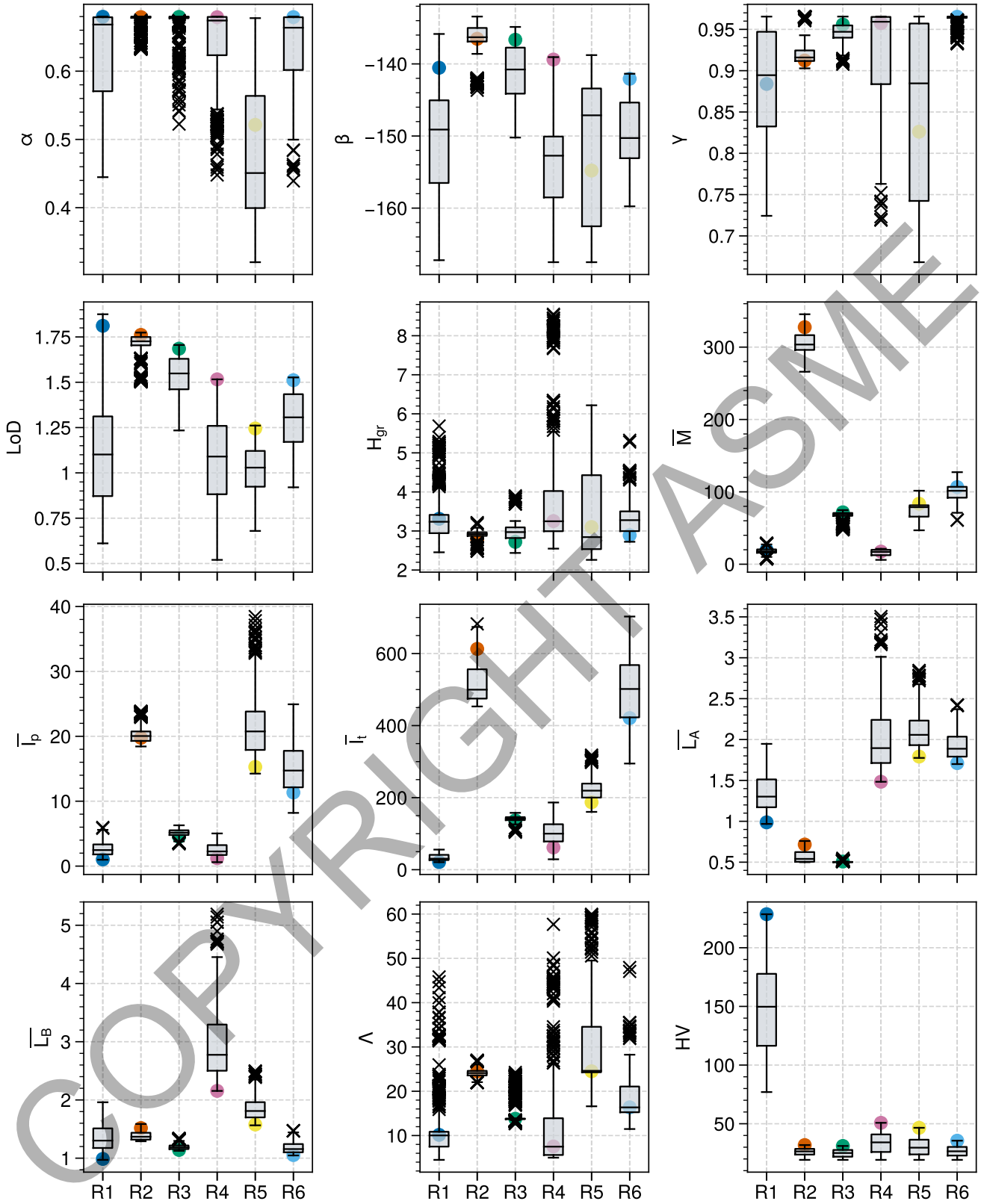

FIGURE 7: BOXPLOTS SHOW THE DISTRIBUTIONS OF DIMENSIONLESS DECISION VARIABLES AND ROBUSTNESS OBJECTIVE *HV* FOR SIX R-OPTIMIZATIONS (R1-R6), WITH MODIFIED ROTOR LENGTH. ROBUST SOLUTIONS FOR EACH OPTIMIZATION ARE OVERLAID IN COLORED SCATTER. HIGHER *HV* VALUES INDICATE GREATER DESIGN ROBUSTNESS TO MANUFACTURING DEVIATIONS.

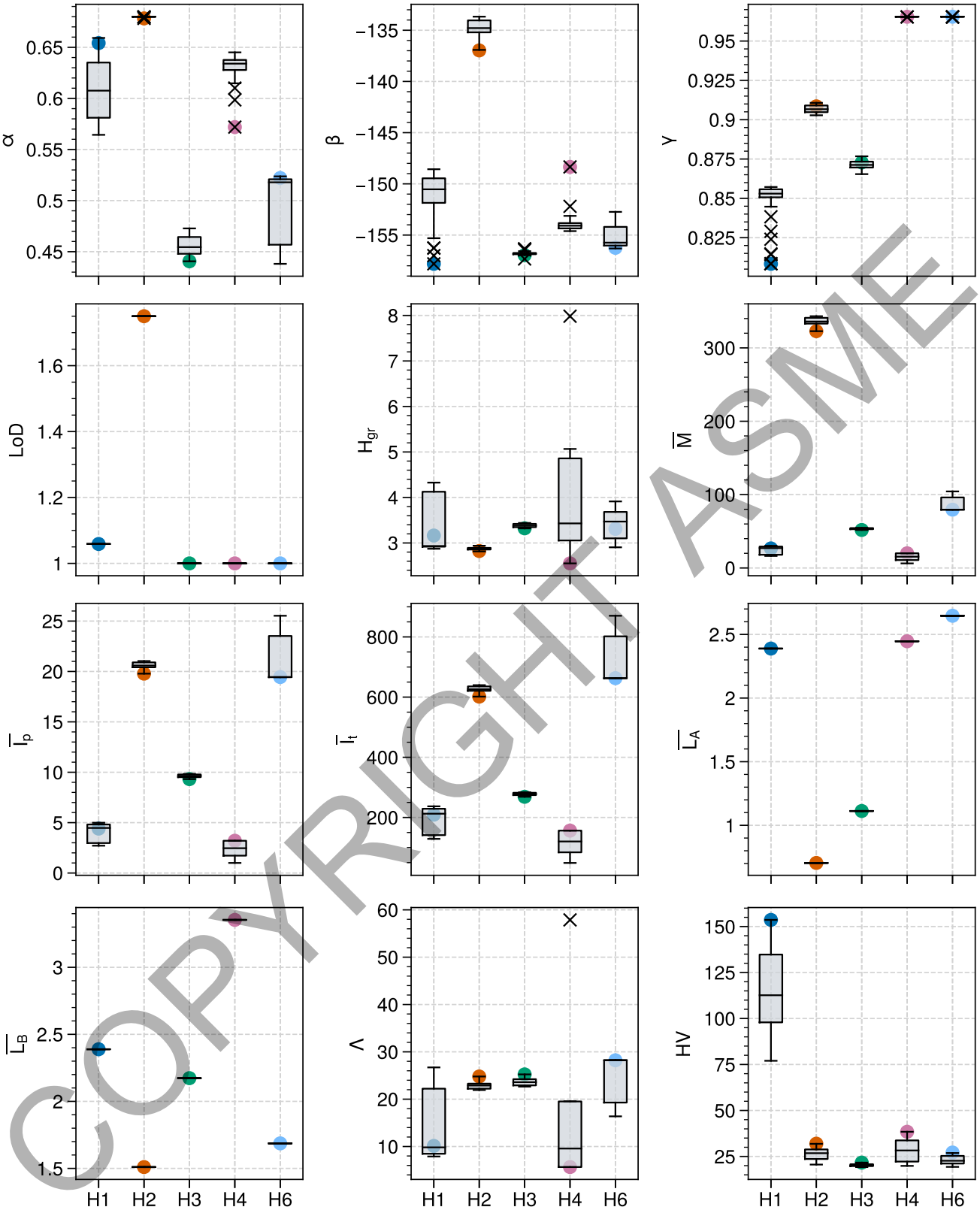

FIGURE 8: BOXPLOTS OF THE DIMENSIONLESS DECISION VARIABLES AND *HV* ROBUSTNESS OBJECTIVE FOR SIX H-OPTIMIZATIONS (H1-H6) ARE SHOWN, WITH H5 OMITTED DUE TO LACK OF SOLUTION. ROBUST SOLUTIONS FOR EACH OPTIMIZATION ARE REPRESENTED BY COLORED SCATTER PLOTS. ONLY BEARING GEOMETRY WAS OPTIMIZED, WHILE SOME VARIABLES (E.G. LoD, $\overline{L_A}$, $\overline{L_B}$) REMAINED FIXED.

A symmetrical rotor design such as $H1_{rob}$ favors a higher value of α. By allowing for the independent selection of both the aspect ratio LoD and the rotor geometry, more robust solutions can be achieved. A bearing aspect ratio in the range of 1.7 to 1.85 seems to be ideal. However, designs such as $R4_{rob}$, $R5_{rob}$, and $R6_{rob}$ were limited by the rotor length constraint and the presence of the fixed-length magnet in between the two bearings, which limited the highest achievable LoD for these designs. The corresponding groove angle β is selected wider at values around $-140°$ to $-134°$. The corresponding groove α values to be selected are all saturated at the upper boundary or 0.68, which means that the groove is two times larger than the ridge. Herringbone grooved journal bearings can be seen as a viscous pump, and adequate combinations of α, β, and LoD allow for proper control of the pressure field in the fluid film. Whilst the influence of γ on bearing performance is not as pronounced as that of α, β, and LoD, the results suggest that selecting values of γ below 1 can improve the robustness of the bearing design. A value of H_{gr} around 3 indicates that a groove depth h_g about twice as large as the local bearing clearance h_r is an ideal ratio for the system to be tolerant to deviations. Equidistant positioning of the centerline of the bearings with respect to the center of gravity of the system is essential for robustness. An ideal rotor design should be symmetrical with a minimal dimensionless mass, polar, and transverse moments of inertia. Furthermore, the dimensionless bearing midplane distance $\overline{L_A}$ or $\overline{L_B}$ to the center of gravity of the system should not be less than but exactly equal to 1. This means that $L_A = L_B = L$, with L being the bearing length. Asymmetry can cause $\overline{L_B}$ to diverge from 1 as $\overline{L_A}$ decreases, leading to less robust designs.

6. CONCLUSION

In this study we presented robustness metrics for the design of gas-bearing supported rotors against manufacturing deviations. Robust designs were formulated as a multi-objective optimization problem under constraints by using sensitivity analysis against manufacturing deviations around the nominal point. A surrogate model made of ensembles of artificial neural networks trained on proper dimensionless numbers for the 4 DOF rotordynamics was used to speed up the computation process. The methodology was successfully applied to six rotor designs for heat pump and fuel cell compressors. Through an analysis of the obtained Pareto fronts, design guidelines were derived for robust herringbone grooved journal bearings against manufacturing deviations.

The results clearly suggest that it is possible to perform robust design via multi-objective optimization of gas-bearings supported rotors in a reasonable time and with widely available computing power. Thanks to the use of an ensemble of artificial networks based surrogate model, each optimization led to accurate results while lasting less than 2h on a modern GPU compared to the hundreds of thousands of CPU core hours required by the baseline model. The selection of robustness metrics, namely the maximization of the feasible region under constraints and the signal-to-noise ratio, has enabled the achievement of stable designs, up to a variation of $\pm 8\,\mu m$ relative to the local bearing clearance. Given the nominal clearance of $10\,\mu m$, this represents a significant improvement in design performance. Analyzing the Pareto optima of the three Pareto fronts, we were able to extract guidelines for the robust design of HGJB supported rotors:

1. The bearing aspect ratio LoD should not be set to 1 but rather around 1.8

2. The groove to ridge width ratio α should be selected around 0.68

3. The bearing groove angle β should have a range from $-140°$ to $-136°$

4. The search of nominal H_{gr} when taking into account centrifugal growth should be in the neighborhood of 3

5. A symmetrical rotor layout is a contributing factor to a robust design by allowing the bearings to be equally distant to the center of gravity. This distance should be equal to the bearing length so that $\overline{L_A} = \overline{L_B} = 1$

This work contributes to a better understanding of the design considerations of herringbone grooved journal bearings in micro-turbocompressors applications. It provides a useful tool for engineers to maximize the robustness of the bearings against manufacturing deviations.

Some limitations are summarized as follows:

1. The analysis is based on predetermined rotor layouts, which were selected to best represent designs encountered in the field of application of micro-turbomachinery for heat pump and fuel cell applications. These layouts facilitate, among others, manufacturing and assembly. There may, however, exist layouts and arrangements that are better suited for robust designs. This is what we attempted to show by introducing a symmetrical rotor without axial bearing or impeller wheel.

2. The optimizations rely on two identical journals, whereas different bearings may have offered better performance in asymmetrical cases.

Future work will focus on extending our analysis by taking into account variability in rotor layouts by positioning the subsystems differently. The constraint of using the same journal bearings for the A-side and the B-side should be relaxed and higher groove-to-ridge width ratios α should be allowed. It may then be necessary to add a constraint on structural integrity of the ridges as well as on the local compressiblity number.

REFERENCES

[1] Schiffmann, J. and Favrat, D. "Design, Experimental Investigation and Multi-Objective Optimization of a Small-Scale Radial Compressor for Heat Pump Applications." *Energy* Vol. 35 No. 1 (2010): pp. 436–450. DOI 10.1016/j.energy.2009.10.010.

[2] Hu, H., Feng, M. and Ren, T. "Effect of Taper Error on the Performance of Gas Foil Conical Bearing." *Industrial Lubrication and Tribology* Vol. 72 No. 10 (2020): pp. 1189–1197. DOI 10.1108/ILT-03-2020-0089.

[3] Moritz G., S., Eifler, T. and Howard, T. J. "Robustness metrics: Consolidating the Multiple Approaches to Quantify Robustness." *Journal of Mechanical Design* Vol. 138 No. 11 (2016): p. 111407. DOI 10.1115/1.4034112.

[4] Zhang, J., Lu, L., Zheng, Z., Tong, H. and Huang, X. "Experimental Verification: a Multi-Objective Optimization Method for Inversion Technology of Hydrodynamic Journal Bearings." *Structural and Multidisciplinary Optimization* Vol. 66 No. 1 (2023): pp. 1–17. DOI 10.1007/s00158-022-03470-z.

[5] Verma, S. K. and Tiwari, R. "Robust Design of Ball Bearings for an Improved Performance Using Genetic Algorithm." *International Journal for Computational Methods in Engineering Science and Mechanics* Vol. 22 No. 6 (2021): pp. 514–537. DOI 10.1080/15502287.2021.1893865.

[6] Guenat, E. and Schiffmann, J. "Multi-Objective Optimization of Grooved Gas Journal Bearings for Robustness in Manufacturing Tolerances." *Tribology Transactions* Vol. 62 No. 6 (2019): pp. 1041–1050. DOI 10.1080/10402004.2019.1642547.

[7] Massoudi, S., Picard, C. and Schiffmann, J. "Robust Design Using Multiobjective Optimisation and Artificial Neural Networks with Application to a Heat Pump Radial Compressor." *Design Science* Vol. 8 (2022): pp. 1041–1050. DOI 10.1017/dsj.2021.25.

[8] Schiffmann, J. and Favrat, D. "The Effect of Real Gas on the Properties of Herringbone Grooved Journal Bearings." *Tribology International* Vol. 43 No. 9 (2010): pp. 1602–1614. DOI 10.1016/j.triboint.2010.03.006.

[9] Vohr, J. H. and Chow, C. Y. "Characteristics of Herringbone-Grooved, Gas-Lubricated Journal Bearings." *Journal of Basic Engineering* Vol. 87 No. 3 (1965): pp. 568–576. DOI 10.1115/1.3650607.

[10] Gu, Lili, Guenat, Eliott and Schiffmann, Jürg. "A Review of Grooved Dynamic Gas Bearings." *Applied Mechanics Reviews* Vol. 72 (2019). DOI 10.1115/1.4044191.

[11] Guenat, E. and Schiffmann, J. "Dynamic force coefficients identification on air-lubricated herringbone grooved journal bearing." *Mechanical Systems and Signal Processing* Vol. 136 (2020). DOI 10.1016/j.ymssp.2019.106498.

[12] Iseli, E. and Schiffmann, J. "Stability and Unbalance Analysis of Rigid Rotors Supported by Spiral Groove Bearings: Comparison of Different Approaches." *Journal of Engineering for Gas Turbines and Power* Vol. 143 No. 12 (2021). DOI 10.1115/1.4052025.

[13] Massoudi, S. and Schiffmann, J. "Ensemble Neural Network Modeling of Gas Bearings Supported Rotors: A Global Surrogate Approach in Multi-Objective Optimization for Robust Design." *Submitted* Vol. 18 (2023).

[14] Ganaie, M. A., Hu, Minghui, Malik, A. K., Tanveer, M. and Suganthan, P. N. "Ensemble deep learning: A review." *Engineering Applications of Artificial Intelligence* Vol. 115 (2022). DOI 10.1016/j.engappai.2022.105151.

[15] He, K., Zhang, X., Ren, S. and Sun, J. "Delving Deep into Rectifiers: Surpassing Human-Level Performance on ImageNet Classification." *2015 IEEE International Conference on Computer Vision (ICCV)*: pp. 1026–1034. 2015. DOI 10.1109/ICCV.2015.123.

[16] Glorot, Xavier and Bengio, Yoshua. "Understanding the difficulty of training deep feedforward neural networks." *Proceedings of the thirteenth international conference on artificial intelligence and statistics*: pp. 249–256. 2010. JMLR Workshop and Conference Proceedings.

[17] LeCun, Yann A, Bottou, Léon, Orr, Genevieve B and Müller, Klaus-Robert. "Efficient backprop." *Neural networks: Tricks of the trade*. Springer (2012): pp. 9–48. DOI 10.1007/978-3-642-35289-8_3.

[18] Papavasileiou, E., Cornelis, J. and Jansen, B. "A Systematic Literature Review of the Successors of "NeuroEvolution of Augmenting Topologies"." *Evolutionary Computation* Vol. 29 No. 1 (2021): pp. 1–73. DOI 10.1162/evco_a_00282.

[19] Deb, K. and Jain, H. "An Evolutionary Many-Objective Optimization Algorithm Using Reference-Point-Based Nondominated Sorting Approach, Part I: Solving Problems With Box Constraints." *IEEE Transactions on Evolutionary Computation* Vol. 18 No. 4 (2014): pp. 577–601. DOI 10.1109/TEVC.2013.2281535.

[20] Jain, H. and Deb, K. "An Evolutionary Many-Objective Optimization Algorithm Using Reference-Point Based Nondominated Sorting Approach, Part II: Handling Constraints and Extending to an Adaptive Approach." *IEEE Transactions on Evolutionary Computation* Vol. 18 No. 4 (2014): pp. 602–622. DOI 10.1109/TEVC.2013.2281534.

[21] Blank, J. and Deb, K. "Pymoo: Multi-Objective Optimization in Python." *IEEE Access* Vol. 8 (2020): pp. 89497–89509. DOI 10.1109/ACCESS.2020.2990567.

[22] Vrugt, J. A. and Robinson, B. A. "Improved Evolutionary Optimization from Genetically Adaptive Multimethod Search." *Proceedings of the National Academy of Sciences* Vol. 104 No. 3 (2007): pp. 708–711. DOI 10.1073/pnas.0610471104.

[23] Hadka, D. and Reed, P. "Borg: An Auto-Adaptive Many-Objective Evolutionary Computing Framework." *Evolutionary Computation* Vol. 21 No. 2 (2013): pp. 231–259. DOI 10.1162/EVCO_a_00075.

[24] Das, I. and Dennis, J. "Normal-Boundary Intersection: A New Method for Generating the Pareto Surface in Nonlinear Multicriteria Optimization Problems." *SIAM Journal on Optimization* Vol. 8 No. 3 (1998): pp. 631–657. DOI 10.1137/S1052623496307510.

APPENDIX A. PLOTS OF THE ROBUST SOLUTIONS FOR FIXED ROTOR GEOMETRY

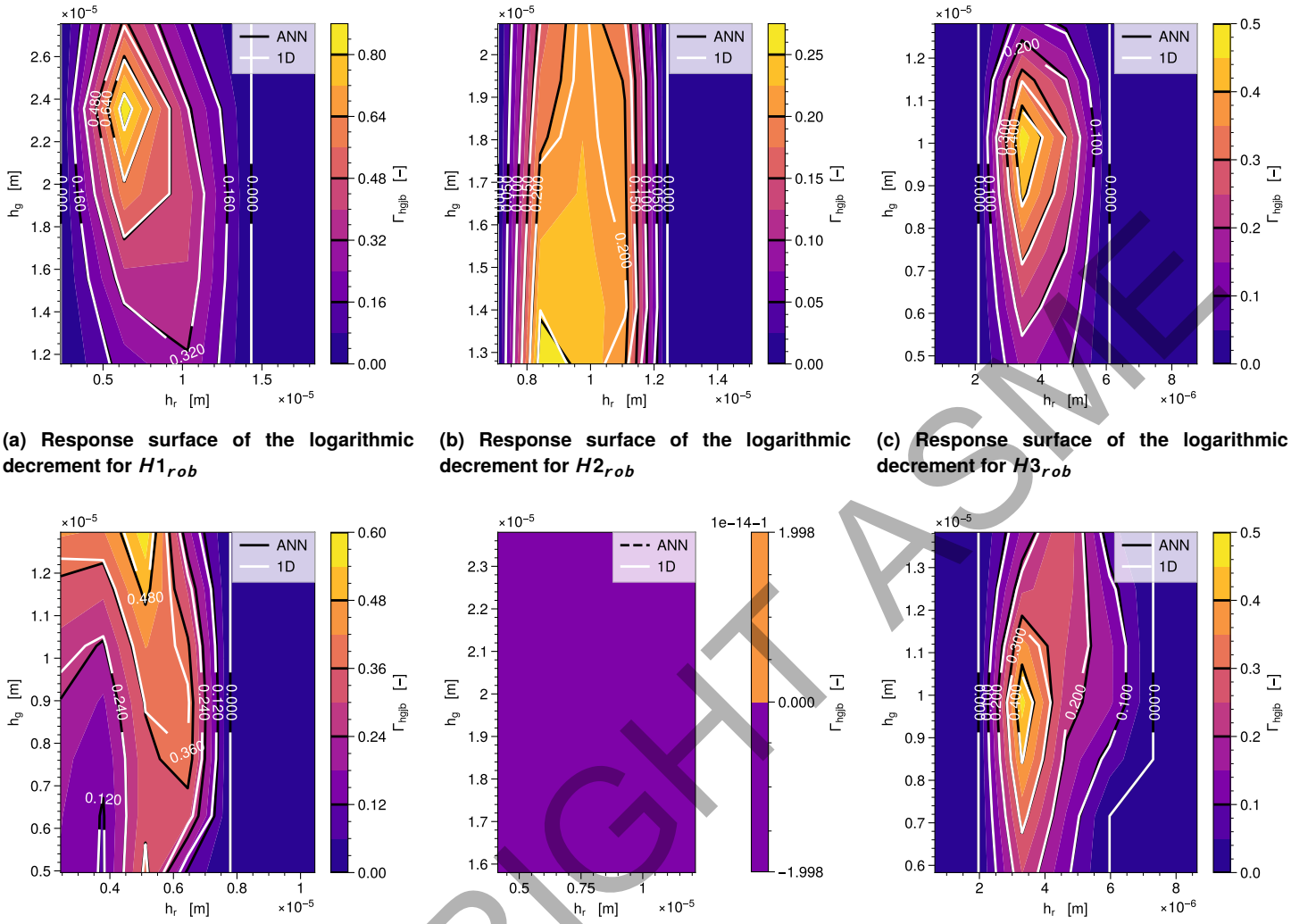

(a) Response surface of the logarithmic decrement for $H1_{rob}$

(b) Response surface of the logarithmic decrement for $H2_{rob}$

(c) Response surface of the logarithmic decrement for $H3_{rob}$

(d) Response surface of the logarithmic decrement for $H4_{rob}$

(e) Response surface of the logarithmic decrement for $H5_{rob}$

(f) Response surface of the logarithmic decrement for $H6_{rob}$

FIGURE 9: RESPONSE SURFACES OF ROBUST SOLUTIONS IN H-OPTIMIZATIONS SHOW THE LOGARITHMIC DECREMENT PLOTTED AS A CONTOUR MAP AGAINST MANUFACTURING DEVIATIONS OF h_r AND h_g. HIGHER TOLERANCES ARE TARGETED FOR h_r, WHICH IS MORE DIFFICULT TO RECTIFY THAN LASER ENGRAVING THE GROOVES. ONLY H1 AND H2 ACHIEVED $\Delta h_r = \pm 2\,\mu m$, AND H5 HAD NO STABLE SOLUTION.